Phase Diagram and Scattering Intensity of Binary Amphiphilic Systems*

G. Gompper and Ulrich S. Schwarz
Sektion Physik der Ludwig-Maximilians-Universität München
Theresienstr. 37, 80333 München, Germany

Z. Phys. B **97**, *233 (1995)*

Abstract

A Ginzburg-Landau model with a scalar and a vector order parameter, which describe the concentration and orientation of the amphiphile, respectively, is used to study the phase diagram and the scattering intensity of binary amphiphilic systems. With increasing amphiphile concentration, the calculated phase diagram shows the typical sequence of ordered phases observed experimentally, that is micellar liquid $\rightarrow$ cubic micellar $\rightarrow$ hexagonal $\rightarrow$ lamellar $\rightarrow$ cubic bicontinuous $\rightarrow$ invers hexagonal. The scattering intensity in the homogeneous phase is calculated in the one-loop approximation. In the vicinity of a phase transition to an ordered phase, the intensity is found to show a $1/q$ behavior for not too small wave vectors q, followed by a small peak, and a $1/q^2$ decay for large wave vectors, in agreement with experimental observations in the L_3- (or sponge-)phase.

PACS numbers: 05.40.+j, 61.20.Gy, 82.70.-y

*Dedicated to Prof. H. Wagner on the occasion of his 60th birthday

1 Introduction

The simplest system, in which the self-assembly of amphiphilic molecules — consisting of a polar head and a non-polar, hydrocarbon tail — can be studied, is a *binary* mixture of non-ionic amphiphiles and water [1, 2, 3]. For example, in binary mixtures of n-alkyl polyglycol ether $C_{12}E_5$ and water [1, 4, 5], with increasing amphiphile concentration the phase sequence

$$\text{micellar liquid } (L_1) \rightarrow \text{hexagonal } (H_I) \rightarrow \text{lamellar } (L_\alpha) \rightarrow \text{cubic}$$

is observed at low temperatures. This sequence can be explained in part by packing constraints [4]. At higher temperatures, two-phase coexistence occurs between a water-rich and an amphiphile-rich phase, which ends in a lower critical point. At still higher temperatures, another isotropic liquid (L_3) is found at very small amphiphile concentration, separated from a highly swollen lamellar phase on one side, and an almost pure water phase on the other side, by first-order phase transitions. The L_3-phase shows quite unusual properties, like a strong flow birefringence, which show that it cannot be another micellar liquid [6, 7]. Freeze-fracture microscopy [8], conductivity and self-diffusion measurements [6, 9, 10, 11, 12] indicate that the structure of this phase consists of a random array of amphiphilic bilayers, which are multiply connected and divide space into two distinct networks of water channels, with a typical separation between the bilayers of the order of 1000 Å [13]. Thus, the L_3- (or sponge-)phase is the analog of the microemulsion phase in ternary amphipilic systems [3].

Among the most important probes of the mesoscopic structure of complex fluids are neutron and light scattering experiments. The scattering intensity of the sponge phase has been calculated in Refs. [14, 15, 16] by assuming that the amphiphilic bilayer forms a perfect two-dimensional surface without any holes or seams. In this case, a unique distinction of water on one side of the bilayer ("inside water") and on the other side ("outside water") can be made. Then, a Ginzburg-Landau model is constructed [14, 15, 16] for *two* scalar order parameter fields, the local concentration difference $\eta(\mathbf{r})$ of inside and outside water, and the amphiphile concentration $\Phi(\mathbf{r})$. With this model, the scattering intensity of a sponge phase is shown to decay as $1/q$ over a range of wave vectors q, where the lower limit is given by the inverse of the correlation length of the η-correlation function (which cannot be measured directly because there is no physical distinction between inside and outside water), and the upper limit by the inverse of the average separation between the bilayers. This power law behavior indeed agrees very well with experimental observations [14, 17, 11, 12].

We want to present in this paper an alternative explanation of the $1/q$ decay of the scattering intensity. We use a Ginzburg-Landau model which takes into account the orientational degrees of freedom of the amphiphile, in addition to the amphiphile concentration [18]. In this model, the bilayer has *not* to be assumed to be perfect. We first show that it reproduces very well the typical sequence of phases which

is observed experimentally with increasing amphiphile concentration. We then calculate the scattering intensity in the homogeneous phase; in the vicinity of a phase transition to an ordered phase, we find that the fluctuations of the amphiphile *orientations* are responsible for a $1/q$ decay, as observed experimentally in the sponge phase.

2 Ginzburg-Landau Model

Our analysis is based on the free-energy functional [18]

$$\begin{aligned}\mathcal{F}\{\Phi,\boldsymbol{\tau}\} = \int d^3r\ \big[&\alpha_1(\nabla\cdot\boldsymbol{\tau})^2+\alpha_2(\nabla^2\boldsymbol{\tau})^2+\alpha_3(\nabla\times\boldsymbol{\tau})^2\\ &+\alpha_4(\nabla(\nabla\cdot\boldsymbol{\tau}))^2+\beta_1(\nabla\Phi)^2+\gamma(\boldsymbol{\tau}\cdot\nabla\Phi)+U(\Phi,\boldsymbol{\tau}^2)\big]\end{aligned} \tag{1}$$

for the scalar order parameter field $\Phi(\mathbf{r})$ and the vector order parameter field $\boldsymbol{\tau}(\mathbf{r})$. Here, Φ is the amphiphile concentration, $\boldsymbol{\tau}/|\boldsymbol{\tau}|$ the amphiphile orientation, and $|\boldsymbol{\tau}|$ the degree of the amphiphile alignment. For the free energy density $U(\Phi,\boldsymbol{\tau}^2)$ we employ the Flory form [18]

$$\begin{aligned}U(\Phi,\boldsymbol{\tau}^2) &= a_2\Phi^2+T\left[\Phi\ln\Phi+M(1-\Phi)\ln(1-\Phi)\right]\\ &+ b_2\boldsymbol{\tau}^2+T\Phi\left[c_2\frac{\boldsymbol{\tau}^2}{\Phi^2}+c_4\frac{(\boldsymbol{\tau}^2)^2}{\Phi^4}\right]\ .\end{aligned} \tag{2}$$

Here, M is the volume of an amphiphile, measured in units of the volume of a water molecule. We have introduced the temperature T as prefactor of the entropic contributions to U in Eq. (2). There is an additional temperature dependence of the interactions, due to the orientational degrees of freedom of the water molecules [19], which we do not take into account.

In a homogeneous phase, the correlation functions in Fourier space,

$$G_{mn}(\mathbf{k}) \equiv 2\int d^3r\ e^{-i\mathbf{k}\cdot\mathbf{r}}\langle\psi_m(\mathbf{r})\psi_n(\mathbf{0})\rangle\ , \tag{3}$$

with $\psi_n=\tau_n$ for $1\le n\le 3$ and $\psi_4=\Phi-\langle\Phi\rangle$, can be calculated quite easily in the Gaussian approximation [18]:

$$\begin{aligned}G^{(0)}_{nm}(\mathbf{k}) &= \frac{\delta_{nm}}{\zeta}-\frac{(\varepsilon-\gamma^2pk^2/4)}{\zeta(\zeta+\varepsilon-\gamma^2pk^2/4)}\frac{k_nk_m}{k^2}\\ G^{(0)}_{4n}(\mathbf{k}) &= -\frac{i}{2}\ \frac{\gamma p}{\zeta(\zeta+\varepsilon-\gamma^2pk^2/4)}k_n=\overline{G^{(0)}_{n4}(\mathbf{k})}\\ G^{(0)}_{44}(\mathbf{k}) &= \frac{p(\zeta+\varepsilon)}{\zeta+\varepsilon-\gamma^2pk^2/4}\ ,\end{aligned} \tag{4}$$

where

$$\begin{aligned}p(k)^{-1} &= \beta_1k^2+\frac{1}{2}\partial^2_\Phi U|_{\Phi=\Phi_0,\boldsymbol{\tau}=\mathbf{0}}\\ \zeta(k) &= \alpha_2k^4+\alpha_3k^2+\frac{1}{2}\partial^2_\tau U|_{\Phi=\Phi_0,\boldsymbol{\tau}=\mathbf{0}}\\ \varepsilon(k) &= \alpha_4k^4+(\alpha_1-\alpha_3)k^2\end{aligned} \tag{5}$$

with $\Phi_0 = \langle\Phi\rangle_0$ being the average amphiphile concentration in the Gaussian approximation. The dependence of the correlation functions (4) on the amphiphile concentration has been discussed in Ref. [18]. In particular, it has been shown that for $\alpha_1 < 0$ and not too small amphiphile concentrations a peak appears at finite wave vector k. This peak signals the self-assembly of the amphiphiles into micelles and bilayers within the homogeneous phase. Note that the scattering intensity $S(k) = \frac{1}{2}\, G_{44}^{(0)}(k)$ decays as k^{-2} for large k in this approximation.

3 Phase Diagram

The phase diagram of a system containing medium-chain amphiphiles is shown in Fig. 1, calculated numerically in the mean-field approximation (MFA) with the same Fourier ansatz and with the same set of parameters as used in Ref. [18]. The value of α_3 is taken to be positive and sufficiently large, so that no phases with a tilt of the amphiphile orientation relative to the layer normal can occur. The phase diagram is identical with the one calculated previously [18], except that we have found another cubic phase (I_1), which is stable in the range $0.15 < \Phi_0 < 0.4$, see Fig. 1. This phase is a FCC crystal of micelles. Its structure can easily be distinguished from the simple cubic V_1-phase, which is bicontinuous, as demonstrated in Fig. 2 by contour plots of both phases. The other cubic structures we have examined, which are the BCC and the single-diamond phases, have been found not to be stable anywhere in the phase diagram. A cut through the phase diagram of Fig. 1 at constant temperature $T = 1.0$ shows that the Ginzburg-Landau model (1) yields *all* ordered phases — in the correct sequence with increasing amphiphile concentration — which are observed in C_iE_j – water mixtures [1, 4]. In particular, the agreement with the phase diagram of the $C_{12}E_8$-plus-water system is quite good.

4 Scattering Intensity

To calculate the scattering intensity in a homogeneous phase beyond the Gaussian approximation, we expand the free-energy functional (1) in powers of $\boldsymbol{\tau}$ and $\tilde{\Phi} \equiv \Phi - \langle\Phi\rangle_0$. To leading order, we find the contributions $\tilde{\Phi}^3$ and $\tilde{\Phi}\boldsymbol{\tau}^2$, so that the free energy functional now takes the form

$$\begin{aligned} \mathcal{F}\{\Phi,\boldsymbol{\tau}\} &= \mathcal{F}_{MFA}\{\Phi_0,\boldsymbol{\tau}=\mathbf{0}\} \\ &+ \int d^3r\, \left[\alpha_1(\nabla\cdot\boldsymbol{\tau})^2 + \alpha_2(\nabla^2\boldsymbol{\tau})^2 + \alpha_3(\nabla\times\boldsymbol{\tau})^2 + \alpha_4(\nabla(\nabla\cdot\boldsymbol{\tau}))^2\right. \\ &\qquad \left. +\beta_1(\nabla\tilde{\Phi})^2 + \gamma(\boldsymbol{\tau}\cdot\nabla\tilde{\Phi}) + r_2\tilde{\Phi}^2 + t_2\boldsymbol{\tau}^2 + \lambda_1\tilde{\Phi}^3 + \lambda_2\tilde{\Phi}\boldsymbol{\tau}^2\right] . \end{aligned} \tag{6}$$

To ensure thermodynamic stability, fourth order terms like $\tilde{\Phi}^4$, $\tilde{\Phi}^2\boldsymbol{\tau}^2$ and $(\boldsymbol{\tau}^2)^2$ are clearly required in the free energy functional. However, they are not necessary for the calculation of the scattering intensity,

and have thus been omitted in Eq. (6). The parameters r_2, t_2, λ_1 and λ_2 of Eq. (6) are related to the parameters of the model (1), (2) by

$$r_2 = \frac{1}{2}\partial_\Phi^2 U|_{\Phi=\Phi_0,\boldsymbol{\tau}=\mathbf{0}} = a_2 + \frac{1}{2}T\left(\frac{1}{\Phi_0} + \frac{M}{1-\Phi_0}\right) \tag{7}$$

$$t_2 = \frac{1}{2}\partial_\tau^2 U|_{\Phi=\Phi_0,\boldsymbol{\tau}=\mathbf{0}} = b_2 + \frac{c_2 T}{\Phi_0} \tag{8}$$

$$\lambda_1 = \frac{1}{6}\partial_\Phi^3 U|_{\Phi=\Phi_0,\boldsymbol{\tau}=\mathbf{0}} = \frac{1}{6}T\left(\frac{M}{(1-\Phi_0)^2} - \frac{1}{\Phi_0^2}\right) \tag{9}$$

$$\lambda_2 = \frac{1}{2}\partial_\Phi \partial_\tau^2 U|_{\Phi=\Phi_0,\boldsymbol{\tau}=\mathbf{0}} = -\frac{c_2 T}{\Phi_0^2} \tag{10}$$

where again $\Phi_0 = \langle\Phi\rangle_0$. Note that the coupling constant λ_2 is always negative, while λ_1 is negative for small Φ_0, but positive for $\Phi_0 > 1/(\sqrt{M}+1)$. The effect of the λ_1-term is to enhance fluctuations of Φ to larger (smaller) values of the local amphiphile concentration for small (large) Φ_0. The λ_2-term acts as a chemical potential for the amphiphile concentration, favoring larger than average amphiphile concentration in regions of large orientational order, *i.e.* inside monolayers. For the calculation of the scattering intensity, we consider r_2, t_2, λ_1 and λ_2 to be phenomenological parameters of our model.

The full correlation functions $G_{mn}(\mathbf{q})$ of model (6) can be expressed exactly in terms of the vertex functions $\Gamma_{ij}(\mathbf{q})$ by the Dyson equation

$$G_{mn}(\mathbf{q}) = \frac{1}{2}\left[G^{(0)}_{mn}(\mathbf{q}) + \sum_{i,j=1}^{4} G^{(0)}_{mi}(\mathbf{q})\Gamma_{ij}(\mathbf{q})G_{jn}(\mathbf{q})\right] \tag{11}$$

which can easily be inverted to give (in matrix form)

$$\mathbf{G}(\mathbf{q}) = \left(\mathbf{1} - \frac{1}{2}\mathbf{G}^{(0)}(\mathbf{q})\boldsymbol{\Gamma}(\mathbf{q})\right)^{-1}\frac{1}{2}\mathbf{G}^{(0)}(\mathbf{q}) \ . \tag{12}$$

In order to proceed, we expand the vertex functions in a series of Feynman diagrams. To leading order in a loop expansion, the vertex functions $\Gamma_{ij}(\mathbf{q})$ are given by the one-loop contributions shown in Fig. 3a. The tadpole diagrams shown in Fig. 3b contribute to the average amphiphile concentration $\langle\Phi\rangle$, which differs from the mean-field value Φ_0. We can now introduce a new variable $\tilde{\psi} = \Phi - \langle\Phi\rangle$, so that $\langle\tilde{\psi}\rangle = 0$. When the free energy functional (6) is written in terms of $\tilde{\psi}$, a *linear* term in $\tilde{\psi}$ appears, which exactly cancels all tadpole contributions to the correlations functions (diagrams containing tadpoles have therefore been omitted in Fig. 3a). At the same time, the coupling constants get renormalized. Since we consider these parameters to be phenomenological anyway, we ignore these corrections here.

In general, the calculation of the Feynman diagrams can only be done numerically. However, in the limit of large surfactant concentrations, where the bare $\tilde{\Phi}\tilde{\Phi}$-propagator vanishes, the dominant contribution can be calculated analytically.

4.1 The Limit of Large Amphiphile Concentrations

In the limit of large amphiphile concentrations $\partial_\Phi^2 U \to \infty$, so that $p \to 0$, see Eq. (5). In this case, the leading contribution comes from the vertex function $\Gamma_{44}(q)$ and is given by

$$\Gamma_{44}(\mathbf{q}) = \frac{\lambda_2^2}{2} \sum_{i,j=1}^{3} \int \frac{d^3k}{(2\pi)^3} G_{ij}^{(0)}(\mathbf{k}) G_{ij}^{(0)}(\mathbf{q}-\mathbf{k}) \ , \tag{13}$$

where the $G_{ij}^{(0)}$ (for $1 \le i,j \le 3$) in this limit reduce to

$$G_{ij}^{(0)}(\mathbf{k}) \to \frac{\delta_{ij}}{\zeta} - \frac{\varepsilon}{\zeta(\zeta+\varepsilon)} \frac{k_i k_j}{k^2} \ , \tag{14}$$

compare Eq. (4). It turns out that the simplest way to calculate Γ_{44} is to use the form

$$\Gamma_{44}(\mathbf{q}) = \frac{\lambda_2^2}{2} \sum_{i,j=1}^{3} \int d^3r \ e^{-i\mathbf{q}\cdot\mathbf{r}} \left[G_{ij}^{(0)}(\mathbf{r}) \right]^2 \tag{15}$$

which is equivalent to (13). Thus, we need the Fourier transform of Eq. (14) to obtain the bare propagators in real space. This calculation is straightforward, so that we immediately give the result:

$$G_{ij}^{(0)}(\mathbf{r}) = \delta_{ij} Q(r) - \partial_i \partial_j W(r) \tag{16}$$

with

$$Q(r) = \frac{1}{8\pi ab\alpha_2} \ \frac{1}{r} e^{-br} \sin(ar) \ , \tag{17}$$

and

$$\begin{aligned} W(r) \ = \ & \frac{1}{2\pi u} \Bigg\{ \frac{1}{r} e^{-br} \left(\alpha_3 (D_x^2 - \alpha_3^2)^{-1/2} \sin(ar) + \cos(ar) \right) \\ & - \frac{1}{r} e^{-dr} \left(\alpha_1 (D_z^2 - \alpha_1^2)^{-1/2} \sin(cr) + \cos(cr) \right) \Bigg\} \ . \end{aligned} \tag{18}$$

The correlation function in real space contains *four* inverse length scales,

$$a = \frac{1}{2} \sqrt{(D_x - \alpha_3)/\alpha_2} \tag{19}$$

$$b = \frac{1}{2} \sqrt{(D_x + \alpha_3)/\alpha_2} \tag{20}$$

$$c = \frac{1}{2} \sqrt{(D_z - \alpha_1)/\alpha_{24}} \tag{21}$$

$$d = \frac{1}{2} \sqrt{(D_z + \alpha_1)/\alpha_{24}} \tag{22}$$

where $\alpha_{24} = \alpha_2 + \alpha_4$, and

$$D_x = \sqrt{2u\alpha_2} \ \ , \ \ D_z = \sqrt{2u\alpha_{24}} \ \ , \ \ u = \partial_\tau^2 U|_{\Phi=\Phi_0, \boldsymbol{\tau}=\mathbf{0}} \ . \tag{23}$$

The function $Q(r)$ has the damped oscillatory form (17) for $-D_x < \alpha_3 < D_x$, whereas it is a sum of two monotonically decaying exponentials for $\alpha_3 > D_x$. Similarly, the function $W(r)$ has the damped

oscillatory form (18) for $-D_z < \alpha_1 < D_z$, whereas it is a sum of four exponentials for $\alpha_1 > D_z$. The lines $\alpha_3 = D_x$ and $\alpha_1 = D_z$ are called disorder lines (DOL) [20, 21, 18]. The oscillatory behavior of the correlation functions indicates that the amphiphile is strong enough to produce a structured fluid. Here, $\alpha_1 < D_z$ is required to describe head-head and tail-tail attraction, and head-tail repulsion; $\alpha_1 = -D_z$ is a spinodal, where the oscillations of the correlation function become long ranged, and a transition to an ordered phase occurs [18]. For the analytic calculation of the scattering intensity, we assume $\alpha_3 < D_x$ for simplicity. There is a tendency for the amphiphiles to tilt with respect to the normal of a monolayer for $\alpha_3 < D_x$, as can be seen, for example, from an oscillatory behavior of the correlation function $\int dx \int dy\, G^{(0)}_{xx}(\mathbf{r})$ [18]. Since we are interested here in systems without tilt, we will take the limit $\alpha_3 \to D_x$ below.

Eq. (16) has now to be inserted into Eq. (15), and the Fourier integral has to be carried out. A few details of this calculation are given in appendix A. Unfortunately, the result of this calculation is rather lengthy, so that the explicit expression is not very enlightning; it is presented in appendix B. However, we can now use the analytic result (29) for the vertex function to derive the power-law behavior of the scattering intensity in the small q limit. In order to describe a highly structured homogeneous system without tilt, we consider the limits $\alpha_1 \to -D_z$, *i.e.* the approach to a spatially ordered phase, and $\alpha_3 \to D_x$. In this case, $a, d \to 0$, and $b, c \to$ const. An expansion of Eq. (29) for small q then yields

$$512\ \pi\ \Gamma_{44}(q) = \lambda_2^2 \frac{1}{c^2 d^3 \alpha_{24}^2} \left(3 + \frac{\alpha_1^2}{u\alpha_{24}}\right)\ \frac{2d}{q} \arctan\left(\frac{q}{2d}\right) + O(q)\ . \tag{24}$$

Thus, for $d < q < c$, the vertex functions shows a $1/q$ decay. Since the bare propagator remains roughly constant in this regime, our model indeed yields the $1/q$ behavior observed experimentally in the sponge phase [14, 17].

For large wave vector q, on the other hand, we obtain from Eq. (29) the asymptotic behavior

$$\Gamma_{44}(q) = O(q^{-2})\ . \tag{25}$$

Thus, the contribution of the bare propagator dominates at large q, which yields a q^{-2} decay, again consistent with experiment.

We expect these results for the q-dependence of the scattering intensity to be valid beyond the limit of very large amphiphile concentrations, or weak coupling between concentration and orientation fields (*i.e.* small coupling constant γ), for the following reasons. First, the general shape of the bare propagator $G^{(0)}_{ij}(\mathbf{q})$ (for $1 \le i, j \le 3$) as a function of the wave vector $\mathbf{q}$ depends only very weakly on $\langle\Phi\rangle_0$ and γ. Second, the most important effect of the one-loop diagrams shown in Fig. 3a is to couple the concentration to the fluctuations of the *orientational* degrees of freedom, independent of the values of $\langle\Phi\rangle_0$ and γ.

4.2 Numerical Results

The effect of the one-loop contributions to the scattering intensity for the system shown in Fig. 1 is rather small, since the coupling constants λ_1 and λ_2 are rather small in the vicinity of the transition to the ordered phases. Eqs. (9) and (10) show that λ_1 and λ_2 become large only for very small amphiphile concentrations. This is in agreement with the experimental observation that the $1/q$-behavior of the scattering intensity occurs in the L_3-phase, a phase which only exists at very low amphiphile concentrations. However, there are no transitions to ordered phases at small Φ_0 for the system of Fig. 1. Other choices of the parameters of model (1), (2) will give other phase diagrams, where ordered phases might occur at lower amphiphile concentrations. In such a case — which we want to consider here — the coupling constants λ_1 and λ_2 of the Ginzburg-Landau model (6) can be considerably larger.

The result of a numerical calculation of the scattering intensity $S(q)$, which includes *all* Feynman diagrams of Fig. 3a, is shown in Fig. 4. The double-logarithmic plot of the data reveals quite clearly that there is a range of q-values, where the scattering intensity falls off almost as $1/q$, and that the decay for large q is as q^{-2}. These two regimes are separated by a small peak, just as observed experimentally in the sponge phase [17]. The general features of the scattering intensity calculated here also agree with those obtained from the "inside-outside" model in Ref. [16]. The main difference of both theroretical results with the experimental data is for wave vectors just beyond the small peak at finite q: While the experiments show a q^{-2} behavior, which sets in right at the peak, the theoretical curves decay considerably faster, see Fig. 4, before they cross over to the asymptotic q^{-2} law.

It has been shown explicitly for the "inside/outside" model of sponge phases that the scattering intensity calculated in the one-loop approximation [16] agrees very well with the result of a Monte Carlo simulation [22]. Therefore, we do not expect higher-order contributions to the vertex functions, which have been omitted from our analysis, to change the qualitative features of the scattering intensity calculated above.

5 Summary and Conclusions

We have studied a Ginzburg-Landau model for binary amphiphilic systems, in which the local amphiphile concentrations and orientations are described by a scalar and a vector order parameter field, respectively. Compared to other Ginzburg-Landau descriptions of binary systems [14, 15, 16, 22], this model has the advantage that it does not require the amphiphile to be assembled in perfect bilayers. Thus, it can describe phases, which are not an ensemble of bilayers, like a cubic crystal of spherical micelles, or a hexagonal packing of cylindrical micelles. In fact, it reproduces very well the typical sequence of phases which is observed experimentally with increasing amphiphile concentration. Furthermore, we have shown

here that the same model also explains the scattering behavior of a strongly structured homogeneous phase at low amphiphile concentrations, where the scattering intensity is characterized by a $1/q$ decay at small wave vector q, followed by a small peak, and a $1/q^2$ behavior for large wave vectors. This is the scattering behavior observed experimentally in the L_3- or sponge-phase. In our calculation, the origin of the $1/q$ behavior is the coupling of the amphiphile concentration to fluctuations of the amphiphile orientation. Since this model has thus been shown to describe the behavior of binary systems very well, it can now be generalized to the case of ternary systems. In particular, it will be interesting to study the evolution of the phase diagram with increasing oil concentration.

Acknowledgements: Helpful discussions with Jürgen Goos are gratefully acknowledged. G.G. thanks the Institute for Theoretical Physics, University of California at Santa Barbara, for its hospitality during the final stages of this work. This work was supported in part by the Deutsche Forschungsgemeinschaft through Sonderforschungsbereich 266, and by the National Science Foundation under Grant No. PHY89-04035.

A Appendix: Some Details of the Calculation of $\Gamma_{44}(\mathbf{q})$

This appendix describes the main steps which are needed to calculate the vertex function $\Gamma_{44}(\mathbf{q})$ from the explicit form of the bare correlation function, Eq. (16). By inserting (16) into (15), one finds

$$\Gamma_{44}(\mathbf{q}) = \frac{\lambda_2^2}{2} \int d^3r \; e^{-i\mathbf{q}\cdot\mathbf{r}} \left[3Q(r)^2 - 2Q(r)\nabla^2 W(r) + \sum_{i,j=1}^{3} \left(\partial_i \partial_j W(r)\right)^2 \right] \; . \tag{26}$$

The last term in Eq. (26) can be rewritten, by repeated integration by parts, in the form

$$\begin{aligned} \int d^3r \; e^{-i\mathbf{q}\cdot\mathbf{r}} \sum_{i,j=1}^{3} \left(\partial_i \partial_j W(r)\right)^2 &= \frac{1}{2} \int d^3r e^{-i\mathbf{q}\cdot\mathbf{r}} \Big[W(r)\nabla^2\nabla^2 W(r) \\ &+ \left(\nabla^2 W(r)\right)^2 + \frac{1}{2} q^4 W(r)^2 + 2q^2 W(r)\nabla^2 W(r) \Big] \; . \end{aligned} \tag{27}$$

This form is advantageous, since

$$\begin{aligned} \nabla^2 \left[\frac{1}{r} e^{-r/\xi} \left(A\sin(qr) + B\cos(qr) \right) \right] &= - \; 4\pi B \; \delta(r) \\ + \frac{1}{r} e^{-r/\xi} \left[\left((\xi^{-2} - q^2)A + \frac{2q}{\xi} B \right) \sin(qr) \right. &+ \left. \left((\xi^{-2} - q^2)B - \frac{2q}{\xi} A \right) \cos(qr) \right] \; . \end{aligned} \tag{28}$$

Thus, the functions $Q(r)$ and $W(r)$ essentially reproduce themselves when the Laplace operator is applied. The resulting integrals can all be expressed by elementary functions [23].

B Appendix: Analytic Expression for Large Amphiphile Concentrations

In the limit $p \to 0$, the analytic expression for the vertex function, Eq. (26), is found to be

$$\begin{aligned} 8\pi\Gamma_{44}(q)/\lambda_2 &= \left(-\frac{1}{\alpha_2} + \frac{q^4}{u} \right) \frac{1}{ub} \; \Lambda_+ \left(\frac{q}{b}, 0, \frac{a}{b} \right) - \left(\frac{1}{\alpha_{24}} - \frac{q^4}{u} \right) \frac{1}{ud} \; \Lambda_+ \left(\frac{q}{d}, 0, \frac{c}{d} \right) \\ &+ \left(1 + \frac{q^4\alpha_3^2}{4u^2} + \frac{\alpha_3^2}{4u\alpha_2} + \frac{q^2\alpha_3}{u} \right) \frac{1}{4a^2b^3\alpha_2^2} \; \Lambda_- \left(\frac{q}{b}, 0, \frac{a}{b} \right) \\ &+ \left(\frac{1}{2} + \frac{q^2\alpha_1}{u} + \frac{q^4\alpha_1^2}{4u^2} + \frac{\alpha_1^2}{4u\alpha_{24}} \right) \frac{1}{4c^2d^3\alpha_{24}^2} \; \Lambda_- \left(\frac{q}{d}, 0, \frac{c}{d} \right) \\ &+ \left(\frac{q^2\alpha_3}{2u} + 1 \right) \frac{q^2}{uab^2\alpha_2} \Xi_+ (\frac{q}{b}, 0, \frac{a}{b}) + \left(1 + \frac{q^2\alpha_1}{2u} \right) \frac{q^2}{ucd^2\alpha_{24}} \; \Xi_+ \left(\frac{q}{d}, 0, \frac{c}{d} \right) \\ &- \left(\frac{q^4\alpha_3\,\alpha_1}{2u} + \frac{\alpha_3\,\alpha_1}{4\alpha_{24}} + q^2\alpha_1 + q^2\alpha_3 + \frac{\alpha_3\,\alpha_1}{4\alpha_2} \right) \\ &\qquad \frac{1}{2uabcd\alpha_2\alpha_{24}(b+d)} \; \Lambda_- \left(\frac{2q}{b+d}, \frac{a-c}{b+d}, \frac{a+c}{b+d} \right) \end{aligned}$$

$$
\begin{aligned}
&+ \left(\frac{1}{\alpha_{24}} - \frac{4q^4}{u} + \frac{1}{\alpha_2}\right) \frac{2}{u(b+d)}\ \Lambda_+\left(\frac{2q}{b+d}, \frac{a-c}{b+d}, \frac{a+c}{b+d}\right) \\
&- \left(q^2 + \frac{\alpha_1}{4\alpha_{24}} + \frac{q^4\alpha_1}{2u} - \frac{\alpha_1}{4\alpha_2}\right) \frac{2}{ucd\alpha_{24}(b+d)}\ \Xi_-\left(\frac{2q}{b+d}, \frac{a-c}{b+d}, \frac{a+c}{b+d}\right) \\
&- \left(\frac{q^4\alpha_3}{2u} + \frac{\alpha_3}{4\alpha_2} + q^2 - \frac{\alpha_3}{4\alpha_{24}}\right) \frac{2}{uab\alpha_2(b+d)}\ \Xi_+\left(\frac{2q}{b+d}, \frac{a-c}{b+d}, \frac{a+c}{b+d}\right) \ .
\end{aligned}
\tag{29}
$$

Here, the functions $\Lambda_\pm$ and $\Xi_\pm$ are defined as

$$
\begin{aligned}
\Lambda_\pm(x,y,z) &= \frac{1}{4x}\Bigg[\arctan\left(\frac{4x}{4+4y^2-x^2}\right) \\
&\qquad \pm \arctan\left(\frac{4x}{4+4z^2-x^2}\right) \pm (m \pm n)\pi\Bigg]
\end{aligned}
\tag{30}
$$

$$
\Xi_\pm(x,y,z) = \frac{1}{8x}\left[\ln\left(\frac{4+(2z+x)^2}{4+(2z-x)^2}\right) \pm \ln\left(\frac{4+(2y+x)^2}{4+(2y-x)^2}\right)\right] \ , \tag{31}
$$

where $n = 0$ for $x^2 < 4(1+y^2)$, while $n = 1$ otherwise, and similarly $m = 0$ for $x^2 < 4(1+z^2)$, while $m = 1$ otherwise.

References

[1] G.J.T. Tiddy, Physics Rep. **57**, 1 (1980).

[2] J. Meunier, D. Langevin, and N. Boccara (eds.), *Physics of Amphiphilic Layers*, Springer Proceedings in Physics **21** (Springer, Berlin, 1987); R. Lipowsky, D. Richter, and K. Kremer (eds.), *The Structure and Conformation of Amphiphilic Membranes* (Springer, Berlin, 1992); W.M. Gelbart, A. Ben-Shaul, and D. Roux, (eds.), *Micelles, Membranes, Microemulsions, and Monolayers* (Springer, Berlin, 1994).

[3] G. Gompper and M. Schick, *Self-Assembling Amphiphilic Systems*, in *Phase Transitions and Critical Phenomena*, Vol. 16, edited by C. Domb and J. Lebowitz (Academic Press, London, 1994).

[4] D. Mitchell, G. Tiddy, L. Waring, T. Bostock, and M. McDonald, J. Chem. Faraday Trans. **79**, 975 (1983).

[5] R. Strey, R. Schomäcker, D. Roux, F. Nallet, and U. Olsson, J. Chem. Soc. Faraday Trans. **86**, 2253 (1990).

[6] G. Porte, J. Marignan, P. Bassereau, and R. May, J. Phys. France **49**, 511 (1988).

[7] M.E. Cates, D. Roux, D. Andelman, S.T. Milner, and S.A. Safran, Europhys. Lett. **5**, 773 (1988).

[8] R. Strey, W. Jahn, G. Porte, and P. Bassereau, Langmuir **6**, 1635 (1990).

[9] D. Gazeau, A.M. Bellocq, D. Roux, and T. Zemb, Europhys. Lett. **9**, 447 (1989).

[10] B. Balinov, U. Olsson, and O. Söderman, J. Phys. Chem. **95**, 5931 (1991).

[11] M. Filali, G. Porte, J. Appell, and P. Pfeuty, J. Phys. II France **4**, 349 (1994).

[12] C. Vinches, C. Coulon, and D. Roux, J. Phys. II France **4**, 1165 (1994).

[13] G. Porte, J. Phys. Cond. Matt. **4**, 8649 (1992).

[14] D. Roux, M.E. Cates, U. Olsson, R.C. Ball, F. Nallet, and A.M. Bellocq, Europhys. Lett. **11**, 229 (1990).

[15] D. Roux, C. Coulon, and M.E. Cates, J. Phys. Chem. **96**, 4174 (1992).

[16] G. Gompper and M. Schick, Phys. Rev. E**49**, 1478 (1994).

[17] M. Skouri, J. Marignan, J. Appell, and G. Porte, J. Phys. II France **1**, 1121 (1991).

[18] G. Gompper and Stefan Klein, J. Phys. II France **2**, 1725 (1992).

[19] J.S. Walker and C.A. Vause, J. Chem. Phys. **79**, 2660 (1983).

[20] M.E. Fisher and B. Widom, J. Chem. Phys. **50**, 3756 (1969).

[21] G. Gompper and M. Schick, Phys. Rev. Lett. **62**, 1647 (1989).

[22] G. Gompper and J. Goos, Phys. Rev. E**50**, 1325 (1994).

[23] I.S. Gradshteyn and I.M. Ryzhik, *Table of Integrals, Series and Products* (Academic Press, San Diego, 1980).

Figure Captions

Figure 1: Phase diagram of a binary system as a function of temperature T and amphiphile concentration $\Phi_0 = \langle\Phi\rangle_0$, calculated from the model (1), (2) with the parameters $\alpha_1 = -6$, $\alpha_2 = 5$, $\alpha_4 = 5$, $\beta_1 = 10$, $\gamma = 30$, $M = 20$, $a_2 = -10$, $b_2 = 1$, $c_2 = 17/12$, and $c_4 = 1$. Continuous phase transitions are shown by dashed lines. The shaded areas are two-phase regions. The full circle denotes a tricritical point.

Figure 2: Contour plots of the order parameter Φ in the I_1- and V_1- phases for constant z. (a) I_1-phase, with $z = 0$; (b) V_1-phase, with $z = 0$; (c) I_1-phase, with $z = 0.25a_0$; (d) V_1-phase, with $z = 0.25a_0$. Here, a_0 is the lattice constant of the cubic structure.

Figure 3: (a) Feynman diagrams, which contribute to one-loop order to the vertex functions $\Gamma_{mn}(\mathbf{q})$. (b) Feynman diagrams ("tadpoles"), which contribute to one-loop order to the average amphiphile concentration, $\langle\Phi\rangle$. Here, the solid lines denote the concentration field $\tilde{\Phi}$, the dashed lines the orientational order parameter $\boldsymbol{\tau}$.

Figure 4: Scattering intensity $S(q) = \frac{1}{2}G_{44}(q)$ of the homogeneous phase, in the vicinity of the spinodal to an ordered phase. The parameters of model (6) are taken to be $\alpha_1 = -6$, $\alpha_2 = 4$, $\alpha_3 = 10$, $\alpha_4 = 4$, $\beta_1 = 16.3$, $\gamma = 21.15$, $r_2 = 5.0$, $t_2 = 8.1$, $\lambda_1 = -32$, and $\lambda_2 = -58$. (a) Linear plot. (b) Double-logarithmic representation.

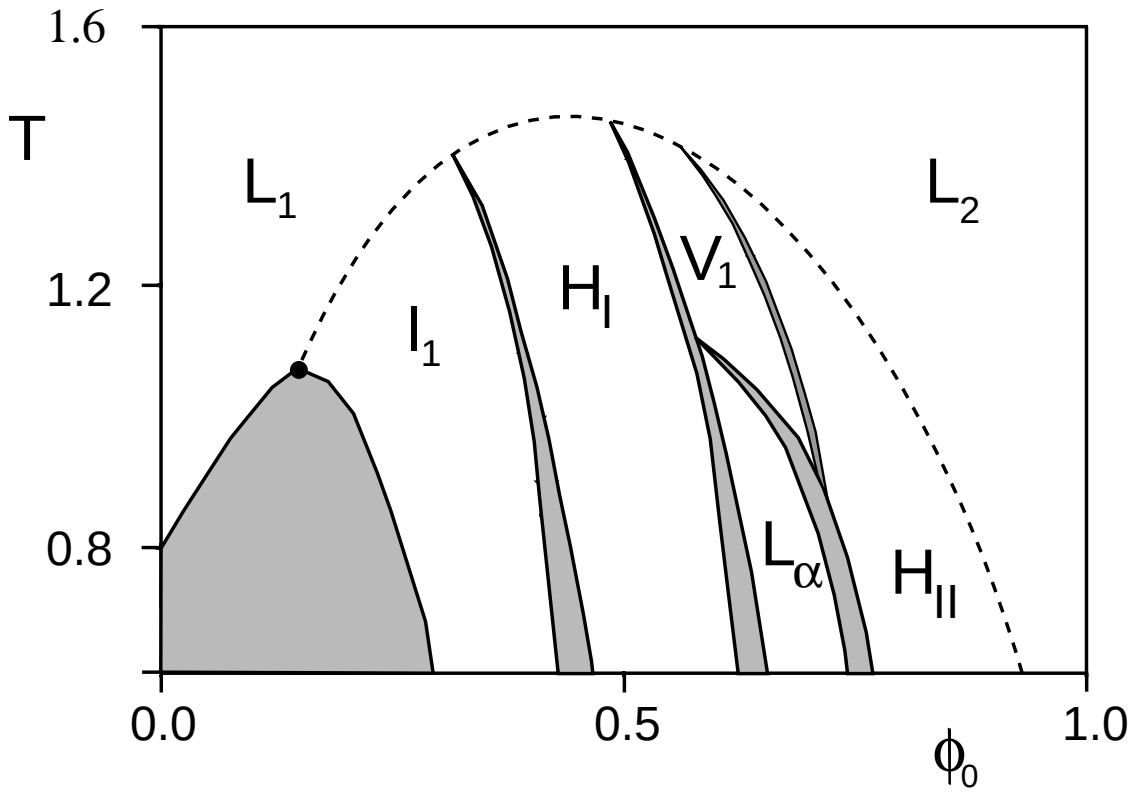

Gompper & Schwarz:
Phase Diagram and Scattering Intensity ...
Figure 1

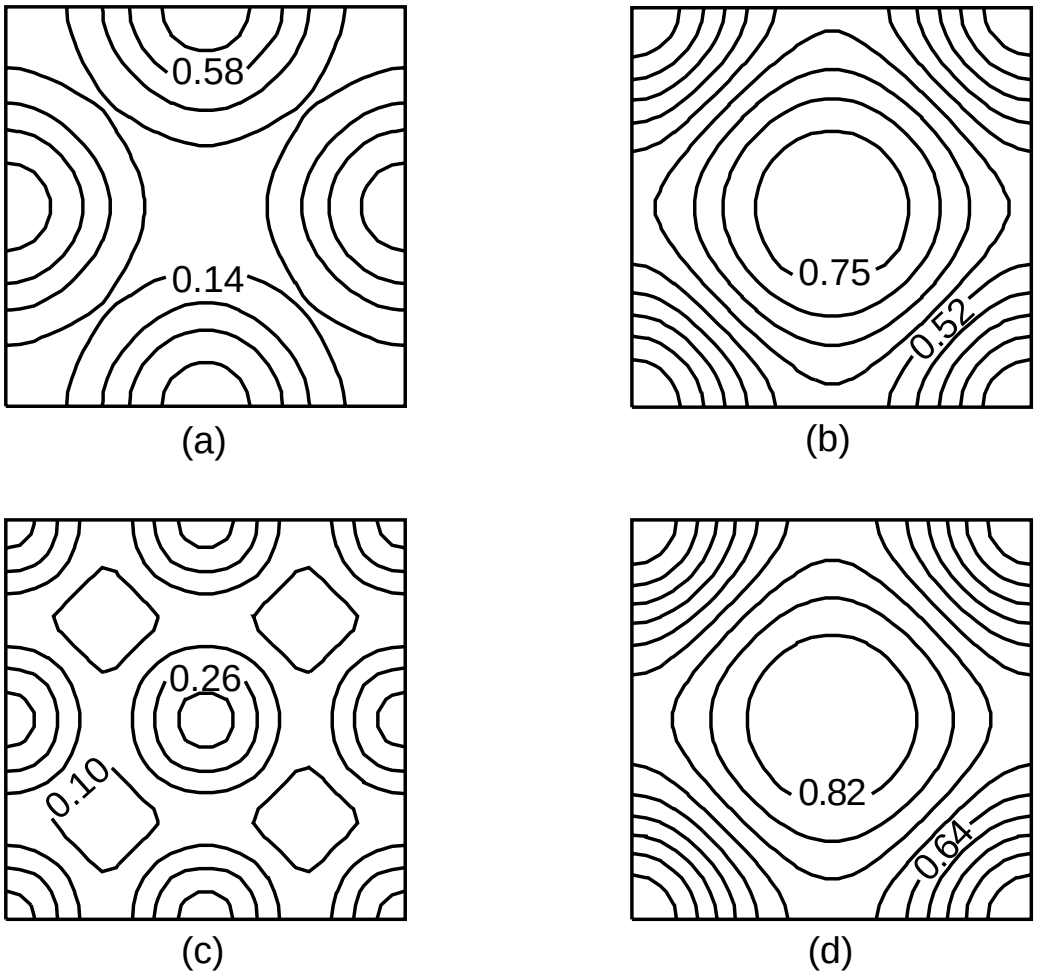

Gompper & Schwarz:
Phase Diagram and Scattering Intensity ...
Figure 2

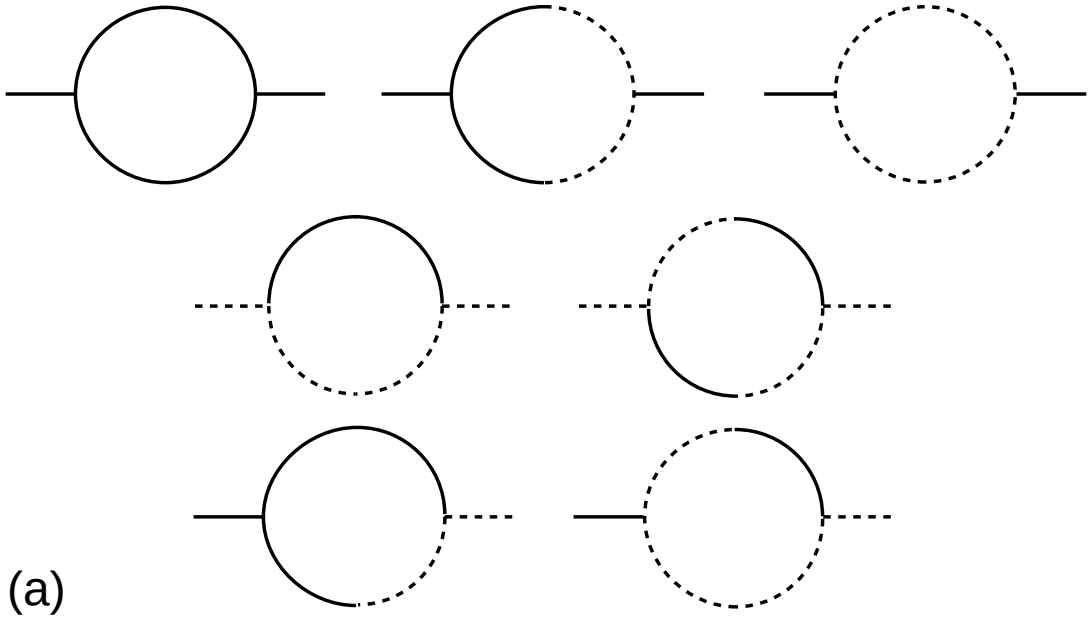

(a)

Gompper & Schwarz:
Phase Diagram and Scattering Intensity ...
Figure 3a

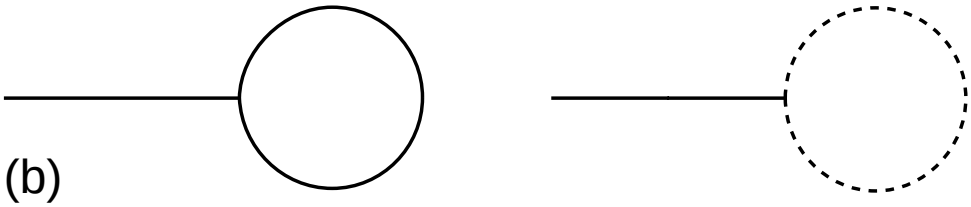

(b)

Gompper & Schwarz:
Phase Diagram and Scattering Intensity ...
Figure 3b

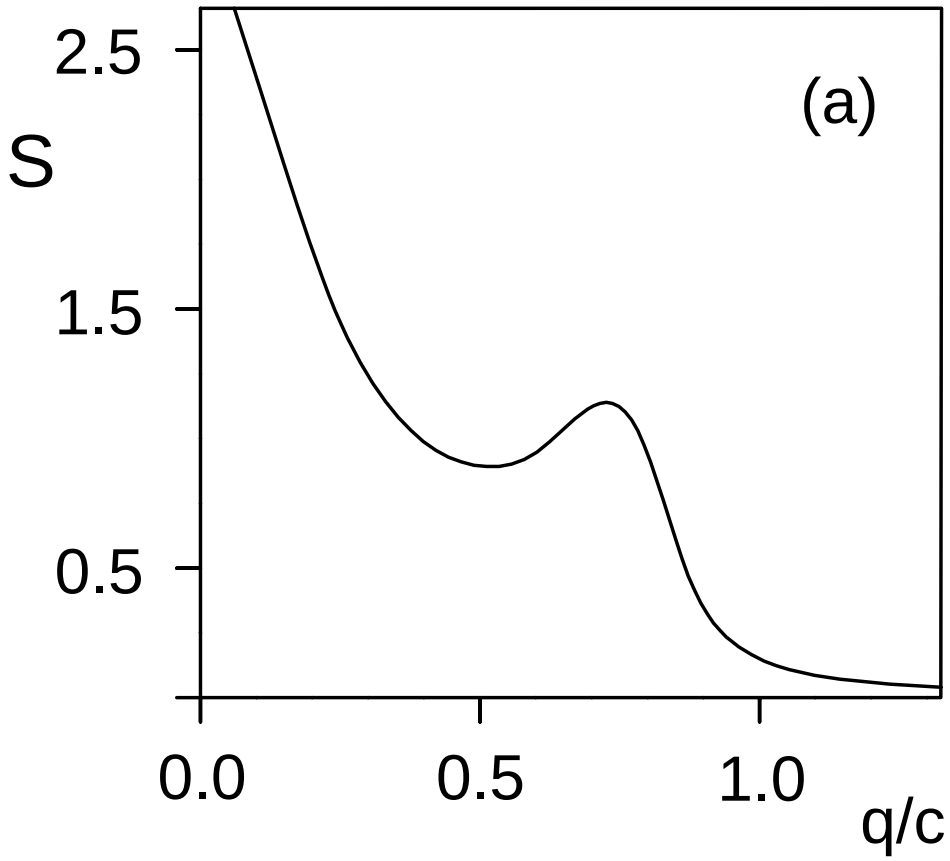

Gompper & Schwarz:
Phase Diagram and Scattering Intensity ...
Figure 4a

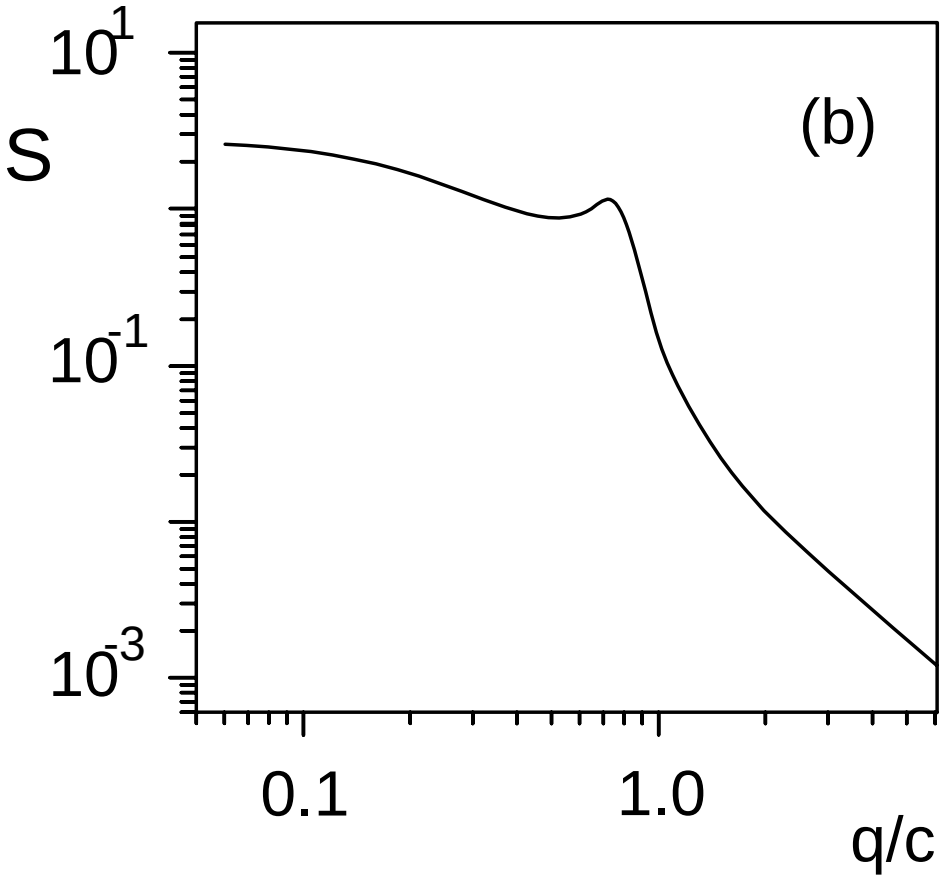

Gompper & Schwarz:
Phase Diagram and Scattering Intensity ...
Figure 4b